J Mol Model (2014) 20:2528
DOI 10.1007/s00894-014-2528-6

ORIGINAL PAPER

Density functional theory calculations insight to the effect of anion on the nonlinear optical properties of $LiInX_2$ (X = S, Se)

Fanjie Kong · Yiliang Liu · Yanfei Hu · Haijun Hou · Feng Hu

Received: 20 August 2014 / Accepted: 10 November 2014 / Published online: 23 November 2014

Abstract The linear and nonlinear optical susceptibilities for $LiInS_2$ and $LiInSe_2$ are studied by density functional theory using total energy pseudo potential plane wave method. The structure, band structure, density of states, and frequency-dependent complex dielectric function $\varepsilon(\omega)$ are calculated. The direct band gap of $LiInSe_2$ is smaller than that of $LiInS_2$. The birefringence Δn (0) is negative for $LiInS_2$ and $LiInSe_2$. The imaginary and real parts of the second-order susceptibility are evaluated. It is found that $\chi^{(2)}_{333}(\omega)$ is the dominant component which shows the largest total Re $\chi^{(2)}_{ijk}(0)$ values. The contribution from the intra-band and inter-band to the second harmonic generation is increased when S is replaced by Se. It is found that a compound with smaller energy band gap has larger values of $\chi_{333}(0)$ which would lead to a possible route to further enhancement of Im $\chi_{333}(\omega)$ by band gap engineering.

F. Kong (✉)
Department of Physics, Yancheng Institute of Technology, Yancheng 224051, People's Republic of China
e-mail: fanjiekong@gmail.com

Y. Liu
College of Electrical and Information Engineering, Southwest University for Nationalities, Chengdu 610041, People's Republic of China

Y. Hu
School of Science, Sichuan University of Science and Engineering, Zigong 643000, People's Republic of China

H. Hou
School of Materials Science and Engineering, Yancheng Institute of Technology, Yancheng 224051, People's Republic of China

F. Hu
School of Mathematic and Physical Science, Xuzhou Institute of Technology, Xuzhou 221008, People's Republic of China

Keywords $LiInS_2$ · $LiInSe_2$ · Linear optical response · Nonlinear optical response

Introduction

Generation of coherent tunable radiation in the mid-infrared (mid-IR 2–20 μm) is of great importance for some applications such as molecular spectroscopy, atmospheric sensing, and various optoelectronic devices. However, only a few suitable nonlinear crystals combining a transparency range extending into the mid-IR above ~5 μm (the upper limit of oxide materials) and large-enough birefringence to permit phase-matching over their transparency ranges are available. The majority of these compounds belong to the ternary chalcogenide semiconductors of the $A^IB^{III}C_2^{VI}$ family, where A = Cu, Ag; B = Al, Ga, In; C = S, Se, Te [1]. Most of the commercially available nonlinear crystals ($AgGaS_2$ or AGS, $AgGaSe_2$ or AGSe, $ZnGeP_2$ or ZGP; GaSe and CdSe) have their advantages and drawbacks. As an example, AGS is transparent from 0.5 up to 13 μm and can be phase-matched over this whole wavelength interval. This material has been recently used for continuous-wave parametric oscillation but it suffers from a low thermal conductivity that reduces the optical damage threshold. Two new materials belonging to the $A^IB^{III}C_2^{VI}$ chalcogenide family, where the metal cations are replaced with the lighter alkali metal (A = Li), can now be added to this limited list. They are biaxial, and allow varying birefringence in a wider range than uniaxial crystals. Compared with other infrared non linear crystals, such as AGS, $LiInS_2$ displays a low anisotropy of linear thermal expansion and a high enough thermal conductivity that is five times greater. These properties are associated with a high damage threshold, which can allow it to be pumped with a high power short pulse laser. Recently, $LiInS_2$ and $LiInSe_2$ crystals with high optical quality became available using the Bridgman–

Stockbarger technique [2, 3] and are applied for second harmonic generation (SHG) and optical parametric oscillation (OPO) in the mid-IR [4]. Lithium alkali metal ternary semiconductors possess excellent properties such as wide transparency range, high nonlinear coefficients, low anisotropy of linear thermal expansion, high enough thermal conductivity and wide opportunities in phase-matching conditions.

Boyd and co-workers first studied $LiInS_2$ and it has attractive optical properties, such as large transparency range from 0.35 to 13 μm and high (estimated at 10.6 μm) nonlinear susceptibility d_{33}=15.8 pm/V in the 70 s [5]. The optical band gap and blue-band emission of $LiInS_2$ single crystal were reported and the band structure nature of $LiInS_2$ was confirmed to be direct with a band gap of 3.73 eV at 77 K [6]. The growth conditions, symmetry, and lattice constants [3] as well as the dielectric coefficients and zone parameters [7] for $LiInSe_2$ were reported. The dispersion of refractive indices in red-phase $LiInSe_2$ crystals was presented and possible nonlinear three-frequency processes in $LiInS_2$ and $LiInSe_2$ crystals used for SHG and OPO were analyzed [8]. The thermal conductivity, thermal expansion and thermo-optic coefficients were measured along the three crystallographic axes of $LiInSe_2$ [9, 10]. By using the local electron density functional with pseudopotentials, Basalaev et al. studied the chemical bonding and electronic structure of chalcopyrite $LiInSe_2$, indicating a donor-acceptor bond peculiarity [11]. Moreover, Li et al. calculated the electronic structures and optical properties of the wurtzite-type $LiInSe_2$, and revealed that $LiInSe_2$ is a good nonlinear semiconductor and the presence of Li cation has a direct influence on neither the band gaps nor the bonding levels but plays an important role in the stabilization of the structures [12]. The structural, electronic, and optical properties of $LiInS_2$ and $LiInSe_2$ have been studied in detail [13]. It was indicated that a strong hybridization between In-5*s*, 5*p* orbits and S-3*p* (Se-4*p*) orbits at upper valence bands is the important structural characteristic of these compounds. Li et al. investigated the structure, electronic properties, optical properties, lattice dynamics, and thermodynamic properties of $LiInSe_2$ polymorph (β-$NaFeO_2$-type, α-$NaFeO_2$-type, and $CuFeS_2$-type), indicating that the α-$NaFeO_2$-type $LiInSe_2$ has the broader density of states, smaller band gap, and special optical properties [14]. The effect of monovalent cations on the electronic, optical, and lattice dynamic properties of $XInSe_2$ (X = Cu, Ag, Li) compounds was investigated. The electronic configurations of X ions, as well as the interactions between X ions and $InSe_4$ groups, are responsible for the different electronic and optical properties of $XInSe_2$ [15]. *Ab initio* investigations of lattice dynamics and thermodynamic properties of $LiInS_2$, $LiInSe_2$, and $LiInTe_2$ revealed that the In–X vibrations are mainly located in the lower frequency range and the Li–X vibrations are dominated in the higher frequency range and the whole lattice vibration spectra move obviously toward the low energy regions on going from $LiInS_2$ to $LiInSe_2$ to $LiInTe_2$ [16]. Brahim Lagoun report *ab initio* study of the elastic and piezoelectric properties of $LiMX_2$ (M = Ga, In; X = S, Se) [17]. When sulfur atoms in ternary chalcogenides are replaced by selenium atoms, the transparency range shifts to longer wavelengths and the nonlinear susceptibility increases by 1.5–2 times [8]. Yet up to now there is no comprehensive work that concerns the electronic structure, frequency dependent dielectric function, birefringence, and frequency dependent nonlinear optical properties of these compounds, although their potential nonlinear optical applications have been emphasized. A comprehensive understanding of the origin of the optical nonlinearity and high $\chi^{(2)}(\omega)$ of these materials are very interesting subjects. For $LiInS_2$ and $LiInSe_2$, the most obvious difference is their anions. Our calculations will focus on the effect of replacing S by Se on the electronic and optical properties.

Computational methods

The ternary $LiInX_2$ (X = S, Se) semiconducting compounds crystallize in β-$NaFeO_2$ structure with orthorhombic space group $Pna2_1$ (point group *mm*2), which presents a distorted superstructure of the wurtzite lattice. Calculations of the noncentro-symmetric semiconductor $LiInS_2$ and $LiInSe_2$ with orthorhombic structure were performed. The lattice constants of compounds were obtained by geometry optimization by the Broyden–Fletcher–Goldfarb–Shanno (BFGS) method [18]. The self consistent norm-conserving pseudopotentials were generated by using FHI98PP code [19] with the Troullier-Martins scheme [20]. Plane waves (PW) were used as basis set for the electronic wave functions. In order to solve the Kohn-Sham equations [21], the conjugate gradient minimization method [22] was employed by the ABINIT code [23]. The exchange-correlation effects were taken into account within the Perdew–Burke–Ernzerhof scheme [24] (PBE) in the generalized gradient approximation (GGA) in the pseudopotential and the band structure calculations. The valence electronic configurations for Li, S, and Se atoms are Li: $2s^1$, S:$3s^2 3p^4$, Se: $4s^2 4p^4$, respectively. For the high localization and full occupation of the *d* orbital of In atom in the compounds, the *d* orbitals were neglected in the In pseudopotential and thus the $5s^2 p^1$ electronic configuration is as the valence electrons [12].

The geometry optimization calculation was obtained with the choice of cutoff energies at 30 Hartree using the 4×3×4 Monkhorst-Pack mesh grid [25]. The band structure calculations took the same Monkhorst-Pack mesh grid for k point sampling. In the linear optical properties calculations, however, the irreducible Brillouin zone (IBZ) has been sampled with 12×9×12 Monkhorst-Pack grid for $LiInX_2$ (X = S, Se). In the nonlinear optical properties, 16×12×16 Monkhorst-Pack grid was used to obtain well converged results.

Results and discussion

Structural properties

The optimized lattice constants along with related theoretical and experimental results for $LiInX_2$ (X = S, Se) are listed in Table 1. Overall, the calculated lattice constants of $LiInX_2$ (X = S, Se) are larger than the experimental ones, which lies in GGA often overestimating lattice constants of solids in general. It can be seen that lattice constants for $LiInS_2$ are in good agreement with the experimental values [26] with deviation of 0.6 % more or less, which is much better than plane wave ultrasoft (UP) and norm-conserving (NC) pseudopotentials calculations using the revised Perdew–Burke–Ernzerhof (RPBE) GGA [13] and the Ceperley–Alder and Perdew–Zunger (CA-PZ) local density approximation (LDA) [16], respectively as exchange-correlation potentials. Meanwhile, the present work overestimates the lattice constants of $LiInSe_2$ by 1.8 % compared with the experimental ones and is consistent with other theoretical findings. The larger lattice constants of $LiInSe_2$ lie in the larger atomic radius than those of the S atom.

Band structure and density of states

The band structures of $LiInX_2$ (X = S, Se) are shown in Fig. 1, which is along the selected Γ-Z-T-Y-S-X-U-R path. It can be seen that the valence band top and the conduction band bottom are located at the Γ point. Therefore, $LiInS_2$ and $LiInSe_2$ are direct semiconductors with a band gap of 2.21 and 1.69 eV, respectively. The decrease of the band gap from $LiInS_2$ to $LiInSe_2$ can be attributed to the shift of the conduction bands toward the Fermi level, which reflects the important role of S in the band gap opening if the valence band is left unchanged. A variety of first-principles approaches previously predicted the direct band gaps of $LiInS_2$ and $LiInSe_2$. For example, the different values are reported to be, 2.46 eV [12], 2.32 eV [13], 3.17 eV [13] for $LiInS_2$ and 1.9 eV [12], 1.79 eV [13], 2.63 eV [13], 2.35 eV [14] for $LiInSe_2$, depending on the calculation methods. The experimentally determined band gaps are determined to be 3.57 eV [27] for $LiInS_2$ and 2.83 eV [27] for $LiInSe_2$. It can be seen that present calculation and others based on DFT all typically underestimate the band gap of $LiInX_2$ (X = S, Se). The discrepancy is due to self-interaction errors and lack of an integer discontinuity of the exchange correlation energy and potential upon changing the number of electrons in the conventional frame work of density functional theory [28]. Meanwhile, the disorder and defects in real crystal also account for the discrepancy of the band gap.

Total density of states (TDOS) along with the Li-2*s*, In-5*s*/5*p*, S-3*s*/3*p*, and Se-4*s*/4*p* partial density of states (PDOS) for $LiInX_2$ (X = S, Se) are shown in Fig. 1. On the whole, they show similar features. In addition, the subtle Li PDOS indicates it can be neglected in the energy range considered, which is consistent with the result reported by [12]. As for PDOS, the valence bands ranging from −12.13 to −10.72 eV and from −12.21 to −11.27 eV comes mostly from S-3*s* and Se-4*s* obitals, respectively and the narrow PDOS curves indicate the S-3*s* and Se-4*s* obitals are localized in $LiInX_2$ (X = S, Se), while the S-3*p* and In-5*s* and the Se-4*p* and In-5*s* orbitals contribute mostly to the σ_{s-p} bonding valence bands from −5.23 to −3.5 eV and from −5.94 to −3.57 eV for $LiInS_2$ and $LiInSe_2$, respectively. The energy ranges from −3.03 eV to the Fermi level and from −3.03 eV to the Fermi level are mainly contributed by the S-3*p* and In-5*p* obitals and the Se-4*p* and In-5*p* orbitals showing σ_{p-p} bonding character. The S-3*p* and In-5*s* obitals and the Se-4*p* and In-5*s* obitals dominate from 2.21 to 4.33 eV and from 2.02 to 3.75 eV in the $(\sigma_{s-p})^*$ antibonding conduction bands for $LiInS_2$ and $LiInSe_2$. The $(\sigma_{p-p})^*$ antibonding conduction bands from 4 to 10 eV are mainly contributed by the S-3*p* and In-5*p* obitals and the Se-4*p* and In-5*p* orbitals. The shift of the antibonding conduction bands to the Fermi level leads to the decrease of the band gap of $LiInSe_2$. The broad distributions of the S-3*p* and Se-4*p* indicate the delocalization of the *p* orbitals of S and Se. The different locations of the S-3*p* and Se-4*p* orbitals in the considered energy range can be attributed to the different energy levels of the S-3*p* and Se-4*p* orbitals (the energy sequence: Se-4*p*<S-3*p*).

Linear optical properties

The optical properties of solids can be described by means of the transverse dielectric function $\varepsilon(\omega)$. These are three principal complex tensor components $\varepsilon^{xx}(\omega)$, $\varepsilon^{yy}(\omega)$, and $\varepsilon^{zz}(\omega)$ for $LiInX_2$ (X = S, Se). The imaginary part of these complex components are $\varepsilon_2^{xx}(\omega)$, $\varepsilon_2^{yy}(\omega)$, and $\varepsilon_2^{zz}(\omega)$. Taking the appropriate transition matrix elements into account, the imaginary part of the dielectric functions $\varepsilon_2(\omega)$ can be calculated [29]. The real part $\varepsilon_1(\omega)$ can be evaluated from $\varepsilon_2(\omega)$ using the Kramer-Kronig relations. The other optical properties, such as the refractive index $n(\omega)$, reflectivity $R(\omega)$, the extinction coefficient $k(\omega)$, and energy-loss spectrum $L(\omega)$ from $\varepsilon_1(\omega)$ and $\varepsilon_2(\omega)$.

In the calculations of the optical properties, a dense mesh of uniformly distributed *k*-points is required. Hence, the Brillouin zone (BZ) integration was performed with 3072*k*-points in the IBZ. Broadening is taken to be 0.1 eV. Our optical properties are scissor corrected by 1.36, 1.14 eV for $LiInS_2$ and $LiInSe_2$, respectively, which is the difference between the calculated and measured energy gap. This could be traced to the fact that GGA calculations usually underestimate the energy gaps. A very simple way to overcome this drawback is to use the scissor correction, which merely makes the calculated energy gap equal to the experimental gap.

Table 1 Theoretical and experimental lattice constants of $LiInS_2$ and $LiInSe_2$

			a (Å)	*b* (Å)	*c* (Å)
$LiInS_2$	GGA-PBE-NC	[a]This work.	6.807[a]	8.232 [a]	6.490 [a]
	Experiment	[b]Ref [26]	6.823[b]	8.266[b]	6.524[b]
	GGA-RPBE-UP	[c]Ref [13]	7.053[c]	8.265[c]	6.626[c]
	GGA-RPBE-NC	[c]Ref [13]	6.777[c]	7.993[c]	6.410[c]
	LDA-CA-PZ-NC	[d]Ref [16]	6.650[d]	7.843[d]	6.298[d]
$LiInSe_2$	GGA-PBE-NC	[a]This work	7.324 [a]	8.567 [a]	6.918 [a]
	Experiment	[b]Ref [26]	7.192[b]	8.412[b]	6.793[b]
	GGA-RPBE-UP	[c]Ref [13]	7.274[c]	8.491[c]	6.980[c]
	GGA-RPBE-NC	[c]Ref [13]	7.122[c]	8.402[c]	6.765[c]
	GGA-PW91-NC	[d]Ref [16]	7.085[d]	8.251[d]	6.751[d]
	GGA-PBE-L/APW+lo	[e]Ref [12]	7.348[e]	8.605[e]	6.933[e]
	LDA-CA-PZ	[f]Ref [14]	7.028[f]	8.237[f]	6.656[f]

The variation of the imaginary (absorptive) part of the electronic dielectric function $\varepsilon_2(\omega)$ is displayed in Fig. 2(a) and (b) for $LiInS_2$ and $LiInSe_2$, respectively. They show similar variation trends and $\varepsilon_2^{xx}(\omega)$, $\varepsilon_2^{yy}(\omega)$, and $\varepsilon_2^{zz}(\omega)$ are anisotropic in the considered energy range. The threshold energy (first critical point) of the dielectric function occurs around band gap. This corresponds to the T_v-T_c splitting which gives the threshold for direct optical transitions between the highest valence and the lowest conduction band. We can see from the figure that $\varepsilon_2(\omega)$ shows a sharp rise after band gap. We define the absorption edge as the energy at which this sharp rise cuts the energy axis. Beyond this point, the curve rises rapidly due to the fact that the number of points contributing toward $\varepsilon_2(\omega)$ increases abruptly. The peaks in the optical response are caused by the electric–dipole transitions between the valence and conduction bands. In order to identify these structures we need to look at the magnitude of the optical matrix elements. The observed structures would correspond to those transitions which have large optical matrix elements. The principle peaks in the spectra are situated around 6.59 eV for $\varepsilon_2^{xx}(\omega)$, $\varepsilon_2^{yy}(\omega)$, and $\varepsilon_2^{zz}(\omega)$ for $LiInS_2$ and 6.11 eV for $LiInSe_2$, respectively in accord with the sequence reported by [13], which are caused by the electron transition between the In 5*p* and the S 3*p* (Se 4*p*) orbitals, respectively. The redshift of the principle peak location for $LiInSe_2$ can be related to its lower energy gap.

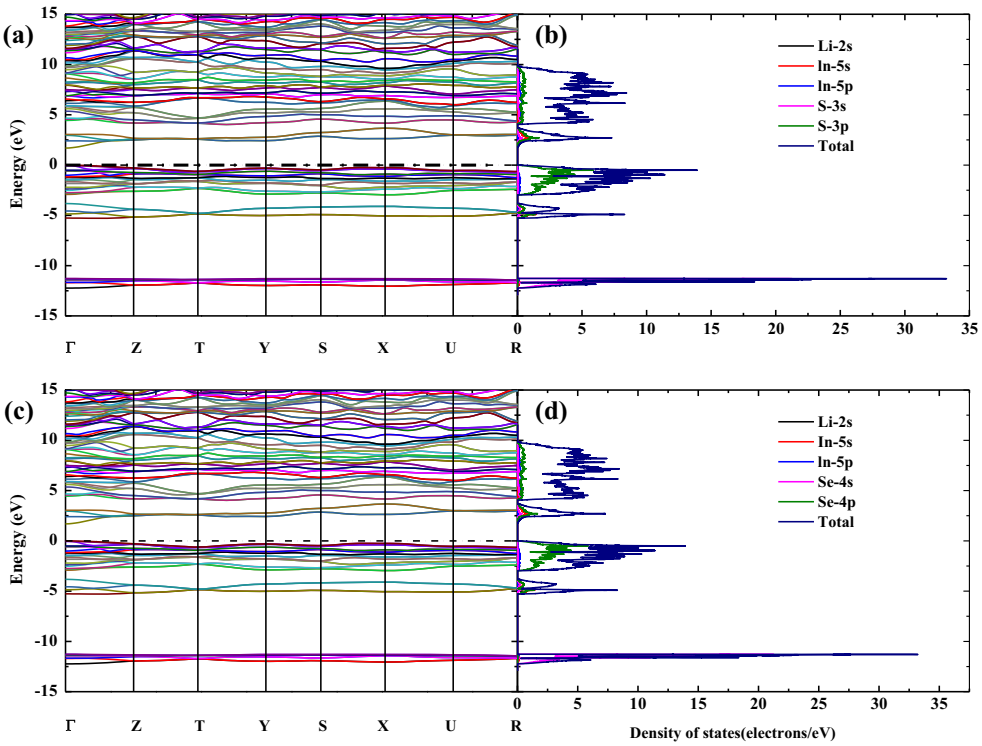

Fig. 1 Band structure of $LiInS_2$ (**a**) and $LiInSe_2$ (**b**), density of states of $LiInS_2$ (**c**) and $LiInSe_2$ (**d**)

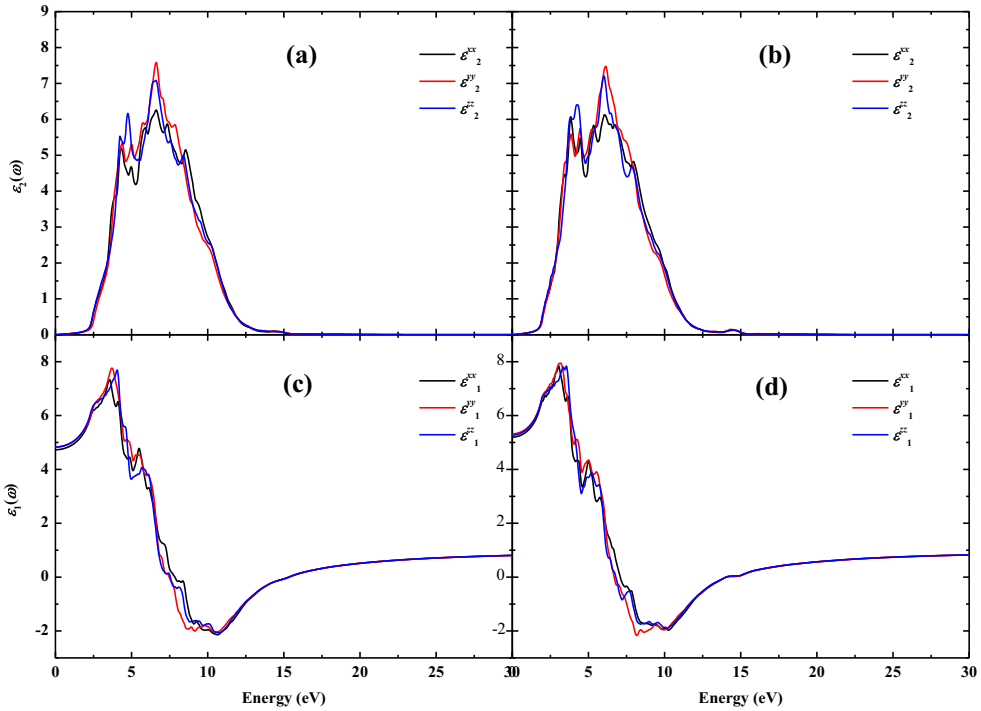

Fig. 2 Linear optical properties of $LiInS_2$ and $LiInSe_2$. **a** Calculated $\varepsilon_2^{xx}(\omega)$, $\varepsilon_2^{yy}(\omega)$, and $\varepsilon_2^{zz}(\omega)$ spectra of $LiInS_2$. **b** Calculated $\varepsilon_2^{xx}(\omega)$, $\varepsilon_2^{yy}(\omega)$, and $\varepsilon_2^{zz}(\omega)$ spectra of $LiInSe_2$. **c** Calculated $\varepsilon_1^{xx}(\omega)$, $\varepsilon_1^{yy}(\omega)$, and $\varepsilon_1^{zz}(\omega)$ spectra of $LiInS_2$. **d** Calculated $\varepsilon_1^{xx}(\omega)$, $\varepsilon_1^{yy}(\omega)$, and $\varepsilon_1^{zz}(\omega)$ spectra of $LiInSe_2$

From the imaginary part of the dielectric function $\varepsilon_2^{xx}(\omega)$, $\varepsilon_2^{yy}(\omega)$, and $\varepsilon_2^{zz}(\omega)$, the real part $\varepsilon_1^{xx}(\omega)$, $\varepsilon_1^{yy}(\omega)$, and $\varepsilon_1^{zz}(\omega)$ are calculated by using the Kramers–Kronig relations. The results of our calculated $\varepsilon_1^{xx}(\omega)$, $\varepsilon_1^{yy}(\omega)$, and $\varepsilon_1^{zz}(\omega)$ spectra are shown in Fig. 2(c) and (d) for $LiInS_2$ and $LiInSe_2$, respectively. The static dielectric constant $\varepsilon_1(0)$ is given by the low energy limit of $\varepsilon_1(\omega)$. Note that we do not include phonon contributions to the dielectric screening, $\varepsilon_1(0)$ corresponds to the static optical dielectric constant (ε_∞). The calculated $\varepsilon_1(0)$ are listed in Table 2. We note that a smaller energy gap yields a larger value. This could be explained on the basis of the Penn model [30], where $\varepsilon(0)$ is related to E_g by the equation $\varepsilon_1(0) \approx 1 + (\hbar\omega_P/E_g)^2$. Hence smaller E_g yields a larger $\varepsilon_1(0)$.

Other optical properties such as refractive index $n(\omega)$, reflectivity $R(\omega)$, the extinction coefficient $k(\omega)$, and energy-loss spectrum $L(\omega)$ can be evaluated. These are illustrated in Fig. 3. Figure 3(a) and (b) display the variation of refractive indices as a function of incident photon energy. We note that at low energy range the investigated materials show high refractive indices and then go to lower values at the high energies. The calculated nonzero tensor components of the static refractive index are 2.175 (2.280) for $n^{xx}(0)$, 2.199 (2.307) for $n^{yy}(0)$, and 2.198 (2.297) for $n^{zz}(0)$ of $LiInS_2$ ($LiInSe_2$). Penn's model shows that $\varepsilon_1(0)$ depends on the energy band gap of the material and $\varepsilon_1(0)$ is directly related to $n(0)$ by the relation $n(0) = (\varepsilon_1(0))^{1/2}$. Figure 3(c) and (d) show the calculated reflectivity spectra. These compounds show low reflectivity at lower energies, which rapidly increases with increasing energies to reach its maximum values at 13.3 (12.5) eV. The absorption bands in the investigated compounds are due to the inter-ion transitions shown in Fig. 3(e) and (f). These figures show that $LiInS_2$ and $LiInSe_2$ single crystals exhibit absorption edges at the fundamental energy gaps and then rapidly increase to reach their maximum at the higher energies. There exists considerable anisotropy between $k^{xx}(\omega)$, $k^{yy}(\omega)$, and $k^{zz}(\omega)$ components at the energy range from 4.29 (3.71) and 10.63 (10.20) eV. Also, we have calculated the electron energy-loss function for $LiInS_2$ and $LiInSe_2$ single crystals, as shown in Fig. 3(g) and (h). The maximum peaks in the energy-loss function are associated with the existence of plasma oscillations.

Figure 4 shows the spectral behavior of the birefringence $\Delta n(\omega)$ for $LiInX_2$ (X = S, Se). Birefringence is important only in the non-absorbing region, which is below the energy gap. The $\Delta n(\omega)$ spectral dependence shows strong oscillations around zero while the birefringence of $LiInSe_2$ show much evident variation in the energy range considered. The calculated birefringence $\Delta n(0)$ is negative with −0.0212 for $LiInS_2$ and −0.0034 $LiInSe_2$, respectively. The birefringence of $LiInX_2$ (X = S, Se) becomes zero beyond 20 eV.

Table 2 The static dielectric constant $\varepsilon_1(0)$

	$LiInS_2$	$LiInSe_2$	
$\varepsilon_1^{xx}(0)$	4.73	5.20	6.24[a]
$\varepsilon_1^{yy}(0)$	4.84	5.32	6.18[a]
$\varepsilon_1^{zz}(0)$	4.83	5.28	6.28[a]

[a] Ref [12]

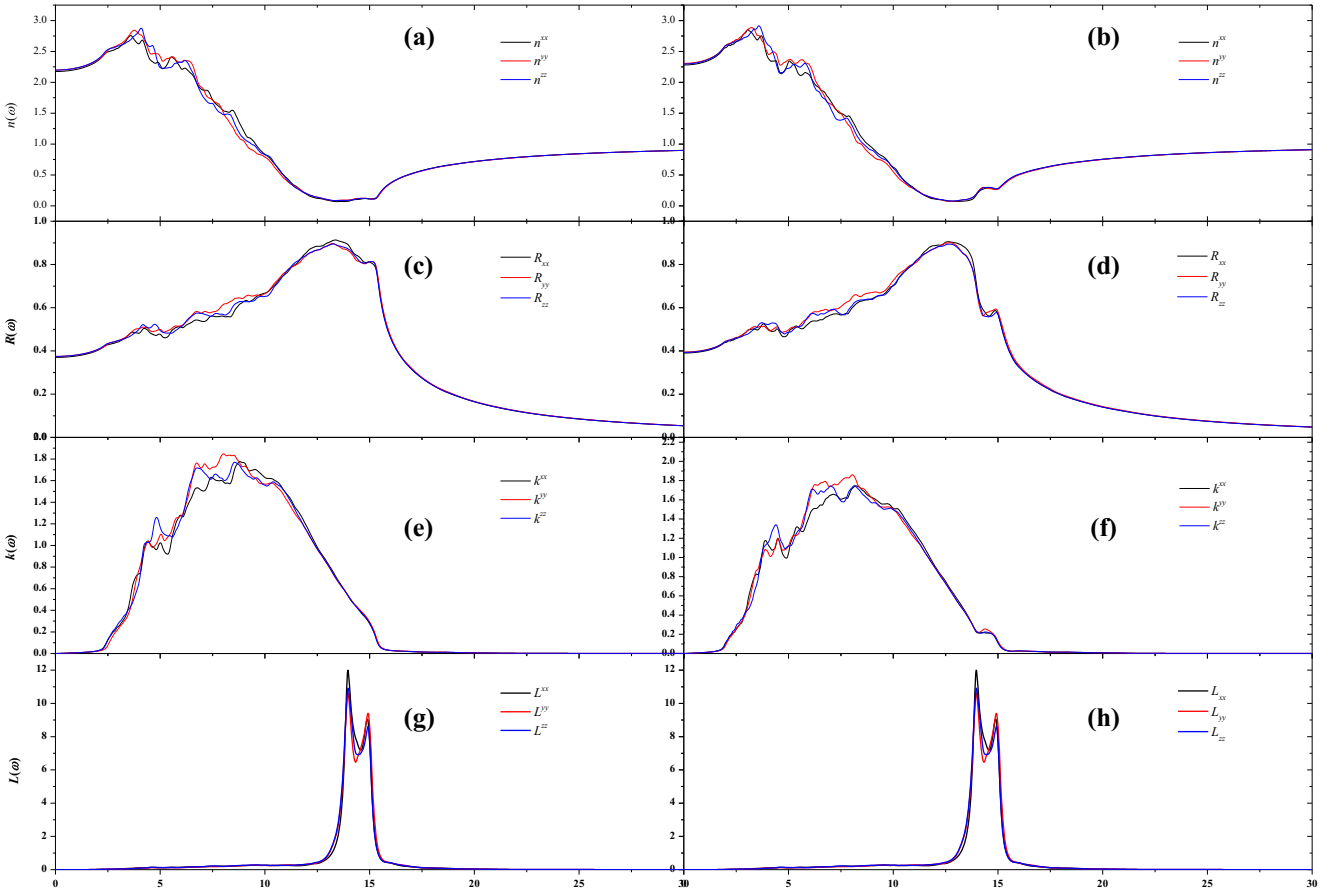

Fig. 3 Calculated refractive indices $n^{xx}(\omega)$, $n^{yy}(\omega)$, and $n^{zz}(\omega)$ for $LiInS_2$ (**a**) and $LiInSe_2$ (**b**), calculated reflectivity indices $R^{xx}(\omega)$, $R^{yy}(\omega)$, and $R^{zz}(\omega)$ for $LiInS_2$ (**c**) and $LiInSe_2$ (**d**), calculated refractive indices $k^{xx}(\omega)$, $k^{yy}(\omega)$, and $k^{zz}(\omega)$ for $LiInS_2$ (**e**) and $LiInSe_2$ (**f**) and calculated energy-loss spectrum $L^{xx}(\omega)$, $L^{yy}(\omega)$, and $L^{zz}(\omega)$ for $LiInS_2$ (**e**) and $LiInSe_2$ (**f**)

Nonlinear optical properties

$LiInS_2$ and $LiInSe_2$ crystallize in the orthorhombic space group $Pna2_1$. Based on this symmetry group there are only three independent components of the SHG third rank polar tensor, namely, the 311, 322, and 333 components (1, 2, and 3 refer to the x, y, and z axes, respectively). For simplicity we write second-order nonlinear optical susceptibility tensor $\chi^{(2)}_{ijk}(-2\omega,\omega,\omega)$ as $\chi^{(2)}_{ijk}(\omega)$ [31]. These are $\chi^{(2)}_{311}(\omega)$, $\chi^{(2)}_{322}(\omega)$, and $\chi^{(2)}_{333}(\omega)$.

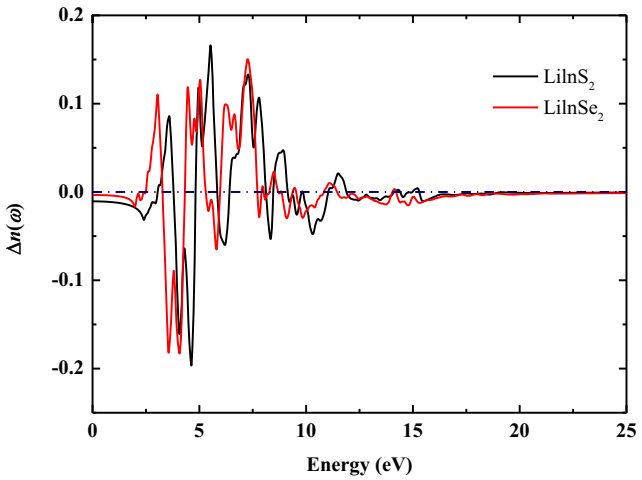

Fig. 4 Calculated birefringence Δn (ω) spectrum for $LiInS_2$ and $LiInSe_2$

The calculated imaginary part of the second-order SHG susceptibilities $\chi^{(2)}_{311}(\omega)$, $\chi^{(2)}_{322}(\omega)$, and $\chi^{(2)}_{333}(\omega)$ of $LiInS_2$ and $LiInSe_2$ are shown in Fig. 5. As can be seen, the total second order susceptibility $\chi^{(2)}_{311}(\omega)$, $\chi^{(2)}_{322}(\omega)$, and $\chi^{(2)}_{333}(\omega)$ determining SHG are zero, below half the band gap. We also show the contributions of ω and 2ω terms. The 2ω term starts contributing at energies ~1/2 E_g and the ω term for energy values above E_g. In the low energy regime (band gap) the SHG optical spectra is dominated by the 2ω contributions. Beyond the values of the fundamental energy gaps the major contribution comes from the ω term.

We have calculated the total complex susceptibility. The real parts are shown in Fig. 6. The lack of experimental data prevents any conclusive comparison with experiment over a large energy range. We find that $\chi^{(2)}_{333}(\omega)$ is the dominant component which shows the largest total Re $\chi^{(2)}_{ijk}(0)$ values of about 0.96 and 1.12 pmV^{-1} for $LiInS_2$ (a) and $LiInSe_2$. It is

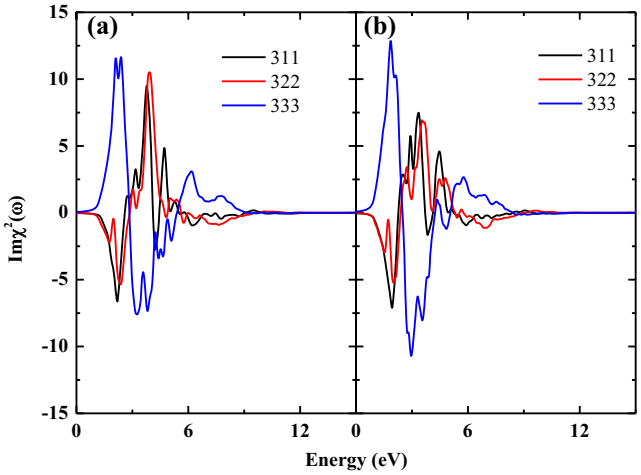

Fig. 5 Calculated Im $\chi^{(2)}_{311}(\omega)$, Im $\chi^{(2)}_{322}(\omega)$, and Im $\chi^{(2)}_{333}(\omega)$ for $LiInS_2$ (**a**) and $LiInSe_2$ (**b**). All Im $\chi^{(2)}(\omega)$ are multiplied by 10^{-7}, in esu units

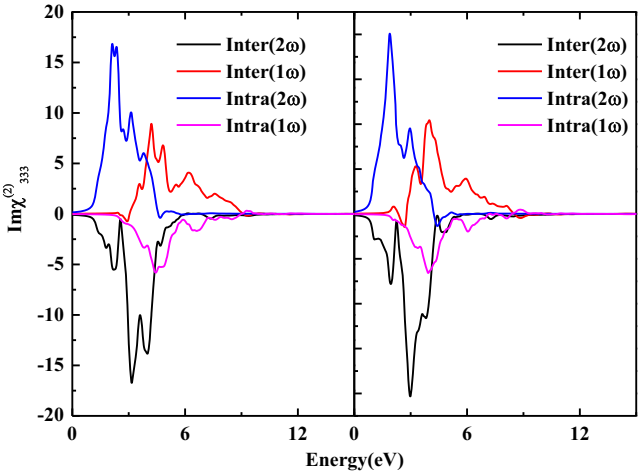

Fig. 7 Calculated total Im $\chi^{(2)}_{333}(\omega)$ spectra along with the intra-$(2\omega)/(1\omega)$ and inter-$(2\omega)/(1\omega)$-band contributions for $LiInS_2$ (**a**) and $LiInSe_2$ (**b**). All Im $\chi^{(2)}(\omega)$ are multiplied by 10^{-7}, in esu units

well known that nonlinear optical susceptibilities are more sensitive to small changes in the band structure than the linear optical ones. Hence any anisotropy in the linear optical properties is enhanced more significantly in the nonlinear spectra.

Figure 7 shows the 2ω and ω inter/intra band contributions to the imaginary parts of $\chi^{(2)}_{333}(\omega)$ for $LiInS_2$ and $LiInSe_2$. Note the opposite signs of the two contributions throughout the frequency range. One could expect that the structures in Im $\chi^{(2)}_{ijk}(\omega)$ could be understood from the features of $\varepsilon_2(\omega)$. Unlike the linear optical spectra, the features in the SHG susceptibility are very difficult to identify from the band structure because of the superposition of 2ω and ω terms. However, we make use of the linear optical spectra to identify the different resonances leading to various features in the SHG spectra. The first spectral band in Im $\chi^{(2)}_{333}(\omega)$ between 1.1 and 2.9 eV (between 0.8 and 2.6 eV) is mainly from the 2ω resonance and arises from the first structure in $\varepsilon_2(\omega)$. The second structure between 2.9 and 5.8 eV (between 2.6 and 5.8 eV) is associated with interference between the ω resonance and 2ω

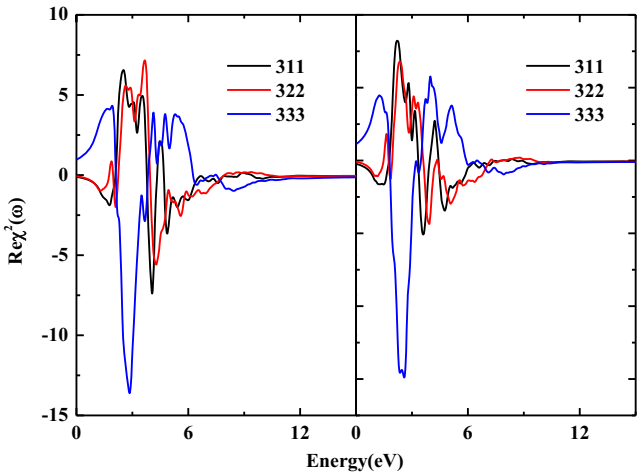

Fig. 6 Calculated Re $\chi^{(2)}_{311}(\omega)$, Re $\chi^{(2)}_{322}(\omega)$, and Re $\chi^{(2)}_{333}(\omega)$ for $LiInS_2$ (**a**) and $LiInSe_2$ (**b**). All Re $\chi^{(2)}(\omega)$ are multiplied by 10^{-7}, in esu units

resonance and it is associated with high energy structure in $\varepsilon_2(\omega)$. The last structure from 5.8 to 9.6 eV (between 5.8 and 9.3 eV) is mainly due to the ω resonance and is associated with the tail in $\varepsilon_2(\omega)$.

In Table 3 we present the values of χ_{333} (0). These values clearly increase on going from S to Se in agreement with experiment and theoretical calculations. We notice that the smaller band gap compounds give higher values of χ_{333} (0) in agreement with the experiment. The lack of experimental data, as well as its contradictory nature, prevents any conclusive comparison with experiment over a large energy range.

Conclusions

We have performed *ab initio* calculations of the structural properties, band structure, density of states, and the linear and nonlinear optical susceptibilities for $LiInX_2$ (X = S, Se) using the pseudo potential method. The lattice constants increase as S is replaced by Se owing to the larger atomic radius of the Se atom. These energy band gaps decrease when S is replaced by Se which can be attributed to the fact that the shift of (σ_{s-p})* antibonding conduction bands toward the Fermi level on going from S to Se . All structures in the imaginary part of the frequency dependent dielectric function $\varepsilon_2(\omega)$ are shifted toward lower energies when S is replaced by Se for $\varepsilon_2^{xx}(\omega)$, $\varepsilon_2^{yy}(\omega)$, and $\varepsilon_2^{zz}(\omega)$. The values of $\varepsilon_1(0)$ increase with the decreasing of the band gap. The birefringence Δn (0) is

Table 3 Experimental and calculated results for $\chi_{333}(0)$. $\chi_{333}(0)$ is expressed in units of pmV^{-1}

	$LiInS_2$	$LiInSe_2$
$\chi_{333}(0)$ exp	31.6[a]	62[b]
$\chi_{333}(0)$ total	40.2	47.1

[a] Ref [4]

[b] Ref [8]

negative for $LiInX_2$ (X = S, Se). Our calculations of SHG susceptibility show that the intra-band and inter-band contributions are significantly increased when S is replaced by Se and smaller band gap materials have higher $\chi_{333}(0)$ values which would lead to a possible route to further enhancement of Im $\chi_{333}(\omega)$ by band gap engineering.

Acknowledgments This project was supported by the Natural Science Foundation of the Higher Education Institutions of Jiangsu Province (Grant nos. 13KJB140018 and 13KJ430007), Jiangsu Overseas Research & Training Program for University Prominent Young & Middle-aged Teachers and Presidents, Natural Science Foundation of China (Grant nos. 11174242, 11204265, and 11474246), Natural Science Foundation of Jiangsu Province (Grant nos. BK2012248 and SBK201342299) and the research fund of Sichuan University of Science and Engineering (Grant nos. 2012PY16, JC-1314 and JG-1404).

References

1. Bhar GC, Smith RC (1972) Phys Status Solidi A 13:157–168
2. Isaenko L, Vasilyeva I, Yelisseyev A, Lobanov S, Malakhov V, Dovlitova L, Zondy JJ, Kavun I (2000) J Cryst Growth 218:313–322
3. Kamijoh T, Kuriyama K (1981) J Cryst Growth 51:6–10
4. Isaenko L, Yelisseyev A, Lobanov S, Petrov V, Rotermund F, Zondy JJ, Knippels GHM (2001) Mat Sci Semicon Proc 4:665–668
5. Boyd GD, Kasper HM, McFee JH (1973) J Appl Phys 44:2809–2812
6. Kuriyama K, Kato T, Takahashi A (1992) Phys Rev B 46:15518–15519
7. Kamijoh T, Nozaki T, Kuriyama K (1982) J Appl Phys 53:761–763
8. Badikov VV, Chizhikov VI, Efimenko VV, Efimenko TD, Panyutin VL, Shevyrdyaeva GS, Scherbakov SI (2003) Opt Mater 23:575–581
9. Yelisseyev AP, Titov AS, Lyapunov KM, Drebushchak VA, Isaenko LI, Lobanov SI (2005) J Cryst Growth 275:e1679–e1684
10. Yelisseyev AP, Drebushchak VA, Titov AS, Isaenko LI, Lobanov SI, Lyapunov KM, Gruzdev VA, Komarov SG, Petrov V, Zondy J-J (2004) J Appl Phys 96:3659–3665
11. Basalaev YM, Zhuravlev YN, Kitova EB, Poplavnoi AS (2007) J Struct Chem 48:1001–1005
12. Li L, Li J, Wu L (2008) J Solid State Chem 181:2462–2468
13. Ma T, Yang C, Xie Y, Sun L, Lv W, Wang R, Zhu C, Wang M (2009) Comp Mater Sci 47:99–105
14. Li Y, Fan W, Sun H, Cheng X, Li P, Zhao X (2009) J Appl Phys 106
15. Li YL, Fan WL, Sun HG, Cheng XF, Li P, Zhao X (2011) J Appl Phys 109:10
16. Ma T, Sun L, Xu C, Chen Y (2011) J Alloy Compd 509:9733–9741
17. Lagoun B, Bentria T, Bentria B (2013) Comp Mater Sci 68:379–383
18. Pfrommer BG, Côté M, Louie SG, Cohen ML (1997) J Comput Phys 131:233–240
19. Fuchs M, Scheffler M (1999) Comput Phys Commun 119:67–98
20. Troullier N, Martins JL (1991) Phys Rev B 43:1993–2006
21. Kohn W, Sham LJ (1965) Phys Rev 140:A1133–A1138
22. Payne MC, Teter MP, Allan DC, Arias TA, Joannopoulos JD (1992) Rev Mod Phys 64:1045–1097
23. Gonze X, Beuken JM, Caracas R, Detraux F, Fuchs M, Rignanese GM, Sindic L, Verstraete M, Zerah G, Jollet F, Torrent M, Roy A, Mikami M, Ghosez P, Raty JY, Allan DC (2002) Comp Mater Sci 25:478–492
24. Perdew JP, Burke K, Ernzerhof M (1996) Phys Rev Lett 77:3865–3868
25. Monkhorst HJ, Pack JD (1976) Phys Rev B 13:5188–5192
26. Isaenko L, Vasilyeva I, Merkulov A, Yelisseyev A, Lobanov S (2005) J Cryst Growth 275:217–223
27. Isaenko L, Yelisseyev A, Lobanov S, Krinitsin P, Petrov V, Zondy JJ (2006) J Non-Cryst Solids 352:2439–2443
28. Jones RO, Gunnarsson O (1989) Rev Mod Phys 61:689–746
29. Reshak AH, Auluck S (2003) Phys Rev B 68:245113
30. Penn DR (1962) Phys Rev 128:2093–2097
31. Rashkeev SN, Lambrecht WRL, Segall B (1998) Phys Rev B 57:3905–3919